Resonant Stellarator Divertor

Alkesh Punjabi[1], Allen Boozer[2]

[1]Hampton University, Hampton, VA 23668, USA

[2]Columbia University, New York, NY 10227, USA

Divertors are required for handling the plasma particle and heat exhausts on the walls in fusion plasmas. There are two basic options for the design of stellarator divertors: non-resonant and resonant [P2.183, A. Punjabi and A. Boozer, 42nd EPS Conference on Plasma Physics, Lisbon, Portugal, June 22-27, 2015]. In non-resonant divertors, external magnetic fields produce a sharp edge where one of the two curvatures of the plasma surface becomes singular along a line. Resonant perturbations produce islands and stochastic regions. The resonant divertors are highly sensitive to the precise value of the rotational transform on the plasma surface. Relatively simple methods are developed to study resonant divertors for stellarators using the field line Hamiltonian. The surfaces that intercept the escaping plasma can have different types of topologies including toroidal, cylindrical, and flat plane. The flat intercepting plane is nonconformal to equilibrium magnetic topology. The effects of the nonideal spiraling and diffusive transport processes on the footprints on the flat plane surfaces are studied. This work is supported by the US DOE grants DE-FG02-01ER54624 and DE-FG02-04ER54793 to Hampton University and DE-FG02-95ER54333 to Columbia University. This research used resources of the NERSC, supported by the Office of Science, US DOE, under Contract No. DE-AC02-05CH11231.

Generally, there are two design options for stellarator divertor designs. The first, dominated by magnetic islands as on W7-X, and second dominated by stochasticity as on LHD. The two designs are based on different principles: islands on the plasma surface for W7-X, called a resonant divertor, and the use of sharp edges on the quasiaxisymmetric stellarator, called the nonresonant divertor [1]. The Hamiltonian equations for the field line are $d\psi_t/d\varphi = -\partial\psi_p/\partial\theta$ and $d\theta/d\varphi = \partial\psi_p/\partial\psi_t$. Position vector for field lines is given by $\vec{x}(\psi_t,\theta,\varphi) = R(\psi_t,\theta,\varphi)\hat{R}(\varphi) + Z(\psi_t,\theta,\varphi)\hat{Z}$. The standard position vector is given by $R = R_a(\varphi) + a\sqrt{\psi_t/\psi_a}\cos\theta, Z = Z_a(\varphi) + a\sqrt{\psi_t/\psi_a}\sin\theta.$ Here we investigate the resonant divertor design option for stellarators with diffusing field lines. We use the NCSX parameters [1]. The total Hamiltonian is $\psi_p(\psi_t,\theta,\varphi) = \overline{\psi}_p(\psi_t) + \widetilde{\psi}_p(\theta,\varphi)$. The unperturbed Hamiltonian

is $\overline{\psi}_P(\psi_t) = a\psi_t + b\psi_t^2$. The perturbation is $\tilde{\psi}_P(\theta,\varphi) = \delta\left[\cos(m_1\theta - n_1\varphi) + \cos(m_2\theta - n_2\varphi)\right]$. The resonant map equations are $\psi_{j+1} = \psi_j + k\delta[\sin(m_1\theta_j - n_1\varphi_j) + \sin(m_2\theta_j - n_2\varphi_j)]$, and $\theta_{j+1} = \theta_j + k\bar{\iota}(\psi_{j+1})$. Both forward and the backward map are used. Resonant perturbation have modes (2,1)+(5,3) with amplitude = 10^{-3}. Both modes are locked with no radial dependence. Footprints are calculated using continuous analogs of forward and backward maps. Lengths of lines, Liapunov lengths, and footprints are calculated. The collecting surfaces are the conformal tori. The safety factor, the equilibrium surfaces, and the phase portrait are shown in Figs.1- 3.

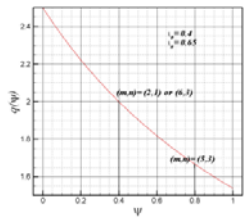

Fig. 1. Equilibrium safety factor for the NCSX.

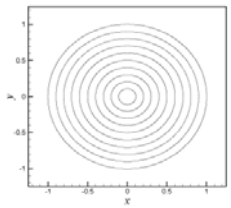

Fig. 2. The equilibrium magnetic surfaces in the NCSX generated by the map.

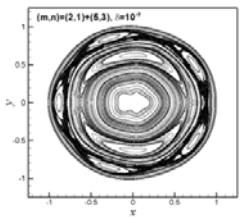

Fig. 3. Phase portrait for the resonant perturbation (m,n)=(2,1)+(5,3) with the amplitude δ=10^{-3} in the φ=0 plane.

For diffusing field lines, the map equations are $\psi_{j+1} \to \psi_{j+1} \pm \Delta\psi_{j+1}$, and $\theta_{j+1} \to \theta_{j+1}$. The $\pm$ sign is chosen at random with equal probability. $\Delta\psi_{j+1}$ is calculated from $\Delta\psi_{j+1} = \left(0.9 + 0.2R_{j+1}\right) D_d / N_p$. R_{j+1} is a random number of uniform density in the range (0,1]. D_d is the average radial displacement per toroidal circuit. D_d is varied from 1E-1 to 1E-5. To calculate footprints from diffusive map equations, the last good surface is calculated and a good surface inside the last good surface is calculated. Fig. 4a shows the Poincare surface of section in the plane φ=0 for the field line trajectories with resonant modes (2,1) + (5,3) of amplitude δ=10^{-3}. The last good surface passes through r=0.93 and θ=0 in the φ=0 plane. Fig. 4b shows an expanded view of Fig. 4a. A good surface inside the last good surface exists passing through r=0.88 and θ=0 in the plane φ=0. Fig. 4c shows the last good surface and the good surface inside the last good surface. The good surface inside the last good surface is made of 10 K points in the φ=0 plane. The good surface serves as the starting position of 10 K field lines. The intersecting surface is the torus of radius r=1. If a field line crosses the intercepting surface, the continuous analog of the map is used to calculate the strike point. If

the line crosses during the application of diffusion operator, simple algebra gives the strike point. Lines are advanced for at most 10 K toroidal transits of the stellarator. If a field line diffusing inwards arrives at a position $r < ½$, the line is thrown away. For D_d =1E-1 to 3E-2, the footprints of the forward and backward lines are a helical loop; and for D_d = 2E-2 to 3E-2, the footprints are a helical curve. For D_d <3E-3, no line strikes the intercepting torus. The typical footprints are shown in Fig. 5. Fig. 5a shows the typical footprint with the structure of a helical loop for D_d=1E-1; and Fig. 5b shows the typical footprint with the structure of a helical curve for D_d=1E-2. The fraction of the 10 K lines starting on the good surface inside the last good surface that strike the intercepting torus in 10 K toroidal transits is denoted by f_s. Fig. 6 shows f_s as a function of D_d. f_s increases with D_d. A third degree polynomial in D_d gives the best fit to the $f_s(D_d)$ data. The area of the footprint is normalized to the area of the intercepting torus of the radius r=1. The normalized area is denoted by A. Fig. 7 shows the area of the footprint as a function of D_d. A cubic polynomial in D_d gives the best fit to the data. So the area A increases with D_d as a cubic polynomial in D_d. The distance traversed by a field line before it strikes the intercepting torus is denoted by l_s. l_s is normalized by the minor radius a. The average length of field lines before they strike, denoted by $<l_s>$, as a function of D_d is shown in Fig. 8. $<l_s>$ scales as $D_d^{-28.88}$ for forward lines and as $D_d^{-28.44}$ for the backward lines. The shortening of the average strike length $<l_s>$ with increasing D_d is very fast. The average Liapunov lengths $<l_L>$ for lines that strike the intercepting surface as function of D_d are shown in Fig. 9. The average Liapunov length decreases much faster as D_d increases when D_d <2E-2 compared to when D_d ≥2E-2. The first region (D_d <2E-2) is when the footprints have the structure of a helical curve while the second region (D_d >2E-2) is when the footprints have the structure of a helical loop. An important finding is that for all the field lines whether moving forward or backward or whether they strike the intercepting surface or not, the average exponential separation is always more than 20 e-folds. This will have significant physics implications for the physics of edge plasmas [2].

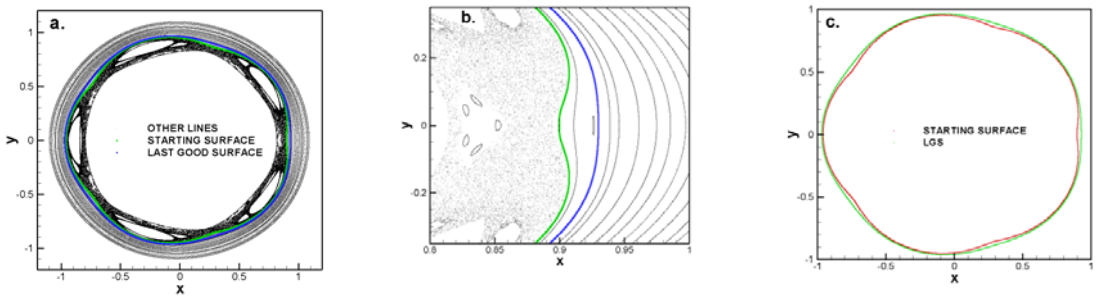

Fig. 4. (a) Phase portrait of field lines in the plane φ=0 from the perturbation (2,1)+(5,3) with amplitude δ=10^{-3}, (b) an expanded view of Fig. 4a showing the last good surface and a good surface passing through r=0.88, θ=0 in the plane φ=0, (c) the last good surface and the starting surface for 10 K field lines inside the last good surface in the φ=0 plane.

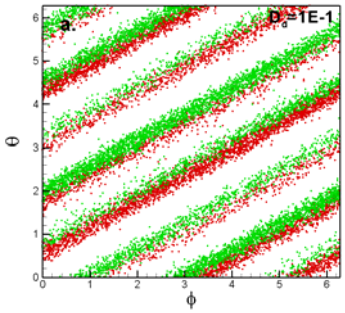

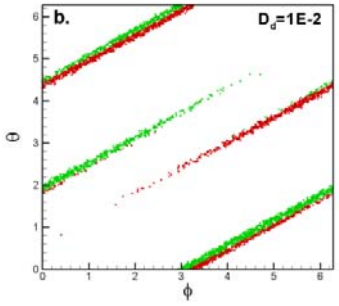

Fig. 5. (a) Footprints for the forward (red) and backward (green) lines when D_d=1E-1. Both the forward and backward footprints have the structure of a helical loop. This structure is typical for D_d=1E-1 to 3E-2, (b) footprints when D_d=1E-2. Both the forward and backward footprints have the structure of a helical curve. This structure is typical for D_d =2E-2 to 3E-3. For D_d<3E-3, there are no footprints.

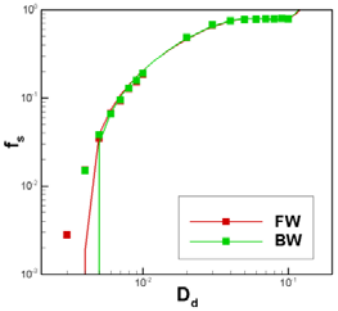

Fig. 6. The fraction f_s of field lines that strike the intercepting surface as a function of D_d. The curve through the data points is a cubic polynomial in D_d fit.

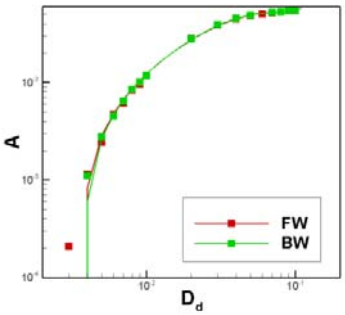

Fig. 7. The normalized area of the footprint, A, on the intercepting torus as a function of D_d. The curve through the data points is a cubic polynomial fit.

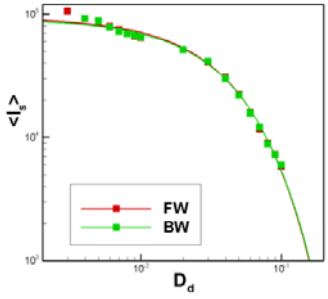

Fig. 8. The average length $<l_s>$ traversed by field lines as a function of D. $<l_s>$ scales as $Dd^{-28.88}$ for forward lines and as $D_d^{-28.44}$ for the backward lines.

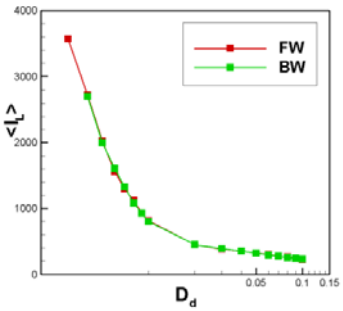

Fig. 9. The average Liapunov length $<l_L>$ as a function of D_d for the lines that strike the intercepting surface.

[1] Design Options for Stellarator Divertors, **P2.183**, A. Punjabi and A. Boozer, 42nd EPS Conference on Plasma Physics, Lisbon, Portugal, June 22-27, 2015

[2] A. H. Boozer, Physics of Plasmas **19**, 112901 (2012)